Article

TfR Aptamer-Functionalized MSNs for Enhancing Targeted Cellular Uptake and Therapy of Cancer Cells

Jiajia Zhang, Jing Shang, Xiuhui Tang,* and Xuemei Xu*

Cite This: *ACS Omega* 2023, 8, 48975−48983

Read Online

ACCESS | Metrics & More | Article Recommendations | Supporting Information

ABSTRACT: Mesoporous silica nanoparticles (MSNs), as novel nano-carriers for drug delivery in cancer treatment, have attracted widespread concern because of their rich pore structure, large pore capacity, ease of modification, and biocompatibility. However, the limitation of nontargeting and low uptake efficiency hindered their further application. Considering the overexpression of the transferrin receptor (TfR) on most cancer cell membranes, herein, we propose a strategy to effectively enhance the cellular internalization of MSNs by arming them with the TfR aptamer. Cellular fluorescent imaging and flow cytometry analysis demonstrated that TfR aptamer-functionalized MSNs exhibited superior cellular internalization compared to unmodified or random sequence-modified MSNs toward three different cancer cell lines, including MCF-7, HeLa, and A549. Furthermore, TfR aptamer-functionalized MSNs displayed enhanced drug delivery efficiency compared with MSNs at equivalent doses and incubation times. These results suggested that TfR aptamer-functionalized MSNs have the potential for enhanced delivery of therapeutic agents into TfR-positive cancer cells to improve therapeutic efficacy.
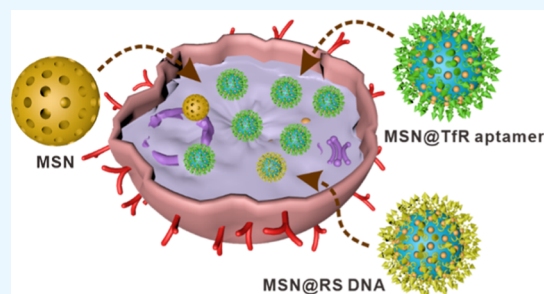
1. INTRODUCTION

Cancer, a malignant disease with high morbidity and mortality, seriously threatens human health.[1,2] Conventional cancer chemotherapy remains challenging because of significant limitations in terms of nonspecific delivery of anticancer drugs, water-insolubility of certain drugs, and severe side effects.[3] With the advancement of nanotechnology, nanomaterials have been utilized as delivery carriers for genes or drugs in recent decades to overcome the limitations associated with traditional drug therapies and attracted continuous attention and in-depth research from materials and medical communities.[4−6] Drugs delivered by nanocarriers can circumvent issues with traditional "free" drug delivery, such as poor solubility, restricted stability, rapid clearance, and especially the lack of targetability. So far, various types of nanocarriers have been developed, including liposomes,[7] polymeric micelles,[8] gold nanoparticles,[9] mesoporous materials,[10] metal−organic frameworks,[11] DNA nanostructures,[12] extracellular vesicles,[13] etc. Among them, mesoporous silica nanoparticles (MSNs) are excellent candidates because of their unique porous structure, large cavities, good biocompatibility, and low cost.[14−17] In addition to physiological stability and controllable drug release performance, compared with other nanocarriers, MSNs can be dispersed in both aqueous and organic phases, especially for water-insoluble drugs, they have highly advantageous loading effects, while approximately 90% of drugs currently used are hydrophobic.[18]

MSNs, as an ideal platform for nanomedicine applications,[19−21] are capable of not only passive targeting by enhancing permeability and retention effects[22] but also active targeting by surface modification of biologically active materials, such as antibodies, peptides, folate, or aptamers.[23−25] In particular, repeated attempts for targeted modification of MSNs using aptamers have been made since they possess advantageous characteristics of low cost, easy accessibility, chemical stability, and low immunogenicity.[26] Besides, studies on the targeted delivery of drugs to cancer cells by means of MSNs modified with aptamers have been published in the last several years. For instance, MUC-1 aptamer-tethered MSNs for ovarian cancer treatment[27] and EGFR aptamer- and chitosan-functionalized MSNs for breast cancer therapy[28] are examples of targeted drug delivery strategies. Nucleolin aptamer-conjugated MSNs for anticancer drug delivery have also been developed to achieve targeted cancer therapy.[29,30] The above examples all demonstrate the feasibility of enhanced targeting drug delivery and cancer treatment by aptamer-functionalized MSNs.
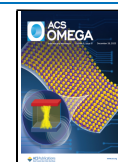
Transferrin receptor (TfR) is a cell-surface-located transmembrane protein involved in intracellular iron transport and typically overexpressed in many cancer cells.[31−33] Studies have
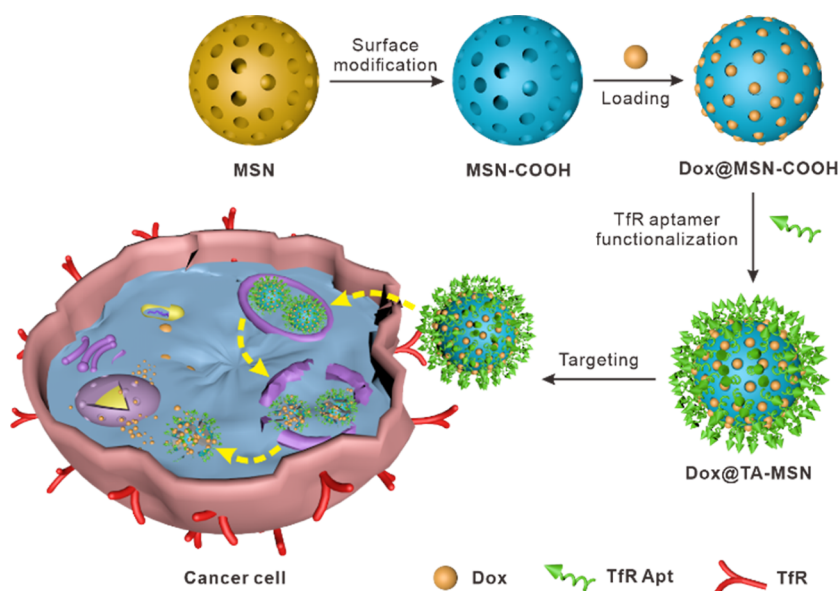
Figure 1. Mechanisms of TfR aptamer-functionalized MSNs for enhanced cellular uptake and drug delivery of cancer cells.

showed that high expression of TfR is associated with increased demand for iron in cancer cells, and it has been an attractive target for targeted delivery in cancer treatment.[34] Recently, TfR aptamers with high affinity toward TfR have been screened, which could readily get inside the cells via clathrin-mediated endocytosis, enabling its use in cancer-targeted therapies.[35−39] Although transferrin-modified MSNs for drug delivery have been previously reported,[40,41] aptamers exhibit more promising clinical applications than proteins because of their advantages of lower cost, more stable chemical properties, easier accessibility, and lower immunogenicity.

Herein, we designed and prepared MSNs decorated with the TfR aptamer (hereinafter referred to as TA), which was reported with high-affinity binding to human tumor cells by Shangguan's group.[38] The TA on the surface of MSNs is beneficial for guiding MSNs to aggregate toward cancer cells and improving the internalization efficiency through surface receptor-mediated endocytosis,[39] as shown in Figure 1. As anticipated, it was found that the TA-functionalized MSNs (TA-MSNs) showed increased targeting efficiency in three cancer cell models, and the Doxorubicin-loaded TA-MSN group exhibited dramatically increased cytotoxicity to cancer cells in comparison to bare MSNs. This is the first attempt and demonstration that TfR aptamer-functionalized MSNs can improve the therapeutic efficiency of human cancer cells, providing a valuable and efficient strategy for developing safer and more universal anticancer therapeutic agents with clinically relevant therapeutic windows.

2. MATERIALS AND METHODS

2.1. Materials. All reagents are commercially available and can be used without any further purification. Tetraethyl orthosilicate (TEOS), hexadecyl trimethylammonium bromide (CTAB), (3-aminopropyl)triethoxysilane (APTES), fluorescein isothiocyanate (FITC), succinic anhydride, potassium bromide, N-hydroxysuccinimide (NHS), N-(3-(dimethylamino)propyl)-N′-ethylcarbodiimide (EDC) hydrochloride, 3-(4,5-dimethylthiazol-2-yl)-2-diphenyltetrazolium bromide (MTT), and magnesium chloride were purchased from Shanghai Aladdin Biochemical Technology Co., Ltd.

Ethanol, dimethyl sulfoxide, and sodium hydroxide were obtained from Sinopharm Chemical Reagent Co., Ltd. Hoechst33342 was purchased from Beyotime Biotechnology (Shanghai, China). DNA oligonucleotides (TfR aptamer NH₂-5′-GGATAGGGATTCTGTTGGTCGGCTGGTTGG-TATCC-3′, random sequence NH₂-5′- AGGATTGATA-CAACCGAGGGCGATCTAACCGCCGA), Doxorubicin (Dox), 30% acrylamide, and TBE buffer were from Sangon Biotech (Shanghai) Co., Ltd. Dulbecco's phosphate buffered saline (PBS), PBS, Dulbecco's modified Eagle's medium (DMEM), MEM, trypsin−EDTA, and penicillin−streptomycin were from Thermo Fisher Scientific (New York, USA). Fetal bovine serum (FBS) was obtained from Hyclone Laboratories, Inc. The human breast cancer cell line (MCF-7), the human cervical carcinoma cell line (HeLa), and the human nonsmall cell lung cancer cell line (A549) were obtained from the Cell Bank of Chinese Academy of Sciences. Ultrapure water (18.2 $M\Omega\cdot cm$, Milli-Q system) was used for all experiments.

2.2. Preparation of MSNs. 110 mL of deionized water and 40 mL of methanol were mixed together, and ammonium hydroxide was added to adjust the pH to 11.24. 0.29 g of CTAB was added and then the mixture was stirred at 1000 rpm and the temperature was raised to 30 °C. Next, 2.5 mL of TEOS was added into the mixture dropwise and stirred for 3 h. After reacting, the mixture was centrifuged at 10,000 rpm for 10 min at room temperature, and the precipitate was washed with ethanol and deionized water three times. After washing, the precipitate was collected and dried in a drying oven, followed by calcining at 500 °C for 6 h to obtain the pure MSNs.

2.3. Preparation of MSN-NH₂. 500 mg of MSN was added into 100 mL of toluene, and the mixture was sonicated for 30 min. Then, 800 µL of APTES was added into the mixture, heated, and reacted at 85 °C for 3 h. After reacting, the mixture was cooled to room temperature and centrifuged at 10,000 rpm for 10 min at low temperature, followed by washing with ethanol three times. After the sample was washed, the precipitate was collected and freeze-dried.

2.4. Preparation of MSN-COOH. 100 mg of MSN-NH₂ was dispersed in 40 mL of ethanol, and 80 mg of succinic
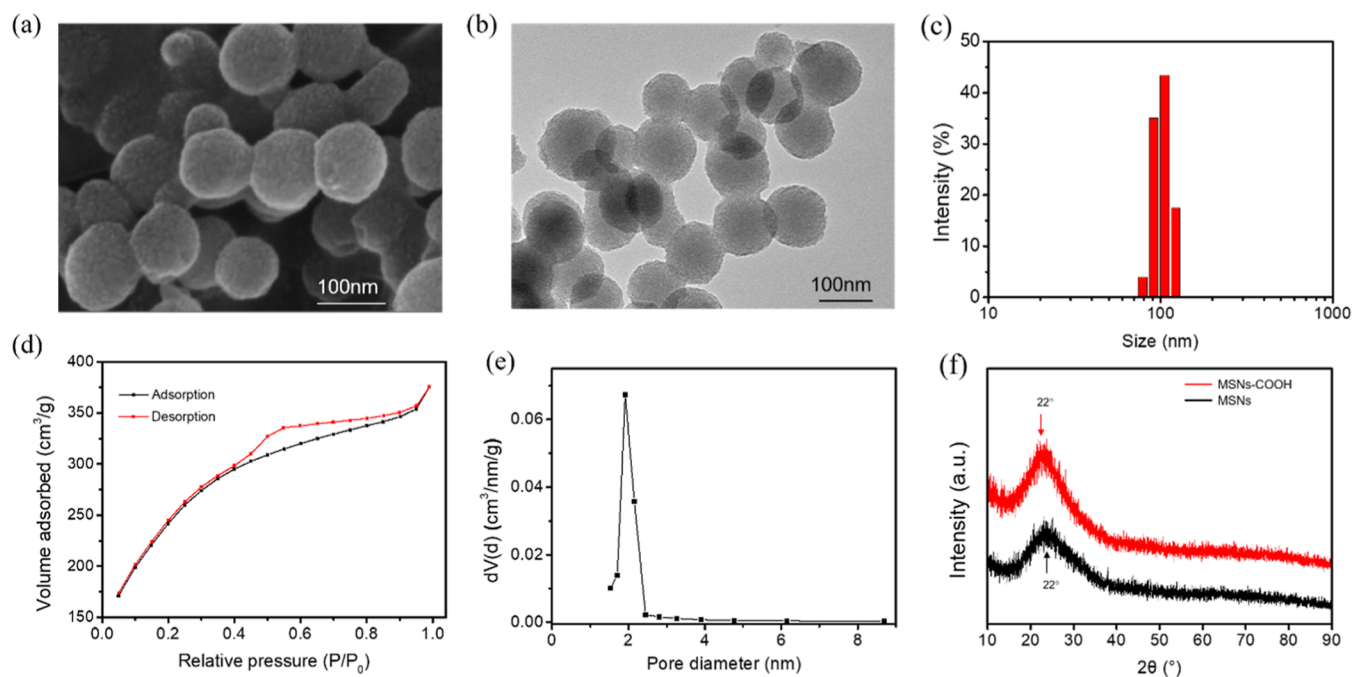
Figure 2. Structural characterization of MSNs. (a) SEM image of MSNs. (b) TEM image of MSNs. (c) Dynamic light scattering measurement of MSNs. (d) Brunauer–Emmett–Teller nitrogen adsorption/desorption isotherms for MSNs. (e) Barrett–Joyner–Halenda pore size distributions for MSNs. (f) XRD characterization of MSNs (black curve) and carboxyl-modified MSNs (red curve).

anhydride was added into it and sonicated for 30 min. The mixture was stirred for 12 h at room temperature. After the reaction, the mixture was centrifuged at 10,000 rpm for 10 min at room temperature and subsequently washed three times each with ethanol and deionized water. After washing, the precipitate was collected and freeze-dried.

2.5. Conjugation of the TfR Aptamer to MSN-COOH. An amino-functionalized TfR aptamer (TfR-NH$_2$) was heated to 95 °C for 5 min and then cooled to room temperature slowly. Next, 50 mg of MSN-COOH, 3 mg of EDC, and 5 mg of NHS were wadded into 10 mL of deionized water and stirred at room temperature for 4 h; then, 10 μL of TfR-NH$_2$ (100 μM) was added into the mixture and stirred for 10 h. After the reaction, the mixture was centrifuged at 10,000 rpm for 10 min at room temperature, followed by washing with deionized water three times. After washing, the precipitate was collected and freeze-dried.

2.6. FITC Loading. For FITC loading, MSN and TA-MSNs (100 mg) were suspended in 10 mL of PBS. Then, the solution of FITC (1 mg, 2.57 μmol) in ethanol (1 mL) was added to the reaction flask, extra PBS was added to the mixture to reach the final volume of 20 mL, and the suspension was stirred for 12 h at room temperature. The loading amount was evaluated by the following equation

$$\text{loading percentage (\%)}$$
$$= \frac{\text{absorption of FITC stock solution} - \text{absorption of supernatant}}{\text{absorption of FITC stock solution}} 100$$

2.7. Dox Loading in Nanocavities. 50 mg of MSNs was mixed with 20 mL of Dox solution (1 mg/mL), and the mixture was stirred for at least 24 h in darkness to achieve the largest loading of Dox. After loading, the above solution was centrifuged (10,000 rpm, 10 min) and the supernatant was discarded. The loading percentage was calculated using the same method as for FITC.

2.8. Drug Release of the Dox@MSNs. To assay the release profiles of Dox, three pH values of 5.4, 6.4, and 7.4 were used for simulation of different biological conditions. 500 μL of buffer-redissolved Dox-loaded nanocarriers were dispersed in 1.5 mL of phosphate (pH = 7.4, 6.4) or citrate buffer (pH = 5.4). Then, the samples were placed in a shaker (0 rpm) at room temperature. The supernatants were taken from the suspension at a given time interval and cleared by centrifugation for monitoring the release of the drug via the fluorescence of Dox. All of the measurements were performed three times. The fluorescence reader was utilized to read the concentrations of Dox (λex = 490 nm; λem = 590 nm).

2.9. Polyacrylamide Gel Electrophoresis. Samples (Aptamer TfR, MSNs, and TA-MSNs) were mixed with loading buffer and loaded on 15% native polyacrylamide gel, and electrophoresis was performed in the 1 × TBE/Mg^{2+} buffer at 110 V for 90 min at 4 °C. After running, the gel was stained with GelRed for 10 min before taking images.

2.10. Cell Culture and Confocal Imaging. MCF-7 and HeLa cells were cultured in high-glucose DMEM with 10% FBS and 1% penicillin–streptomycin at 37 °C under a 5% CO$_2$ atmosphere. A549 cells were cultured in modified Eagle's medium with 10% FBS and 1% penicillin–streptomycin at 37 °C under a 5% CO$_2$ atmosphere. For fluorescent imaging, cancer cells (2.5×10^4) were seeded on a confocal culture dish and attached for 24 h. FITC@MSN, FITC@RS-MSN, and FITC@TA-MSN samples were added into the dish to make the final concentrations 0, 10, 50, 100, and 200 μg/mL and incubated with cancer cells for 4 h, followed by PBS washing three times. The cell nuclei were stained with 1 μg/mL Hoechst33342 for 10 min before laser scanning-confocal microscopy (FV 1000 Olympus) imaging measurements.

2.11. Flow Cytometry Assay. Flow cytometry analysis was performed to evaluate the cellular uptake of nanoparticles. Cancer cells (2.0×10^4) were cultivated in 96-well culture
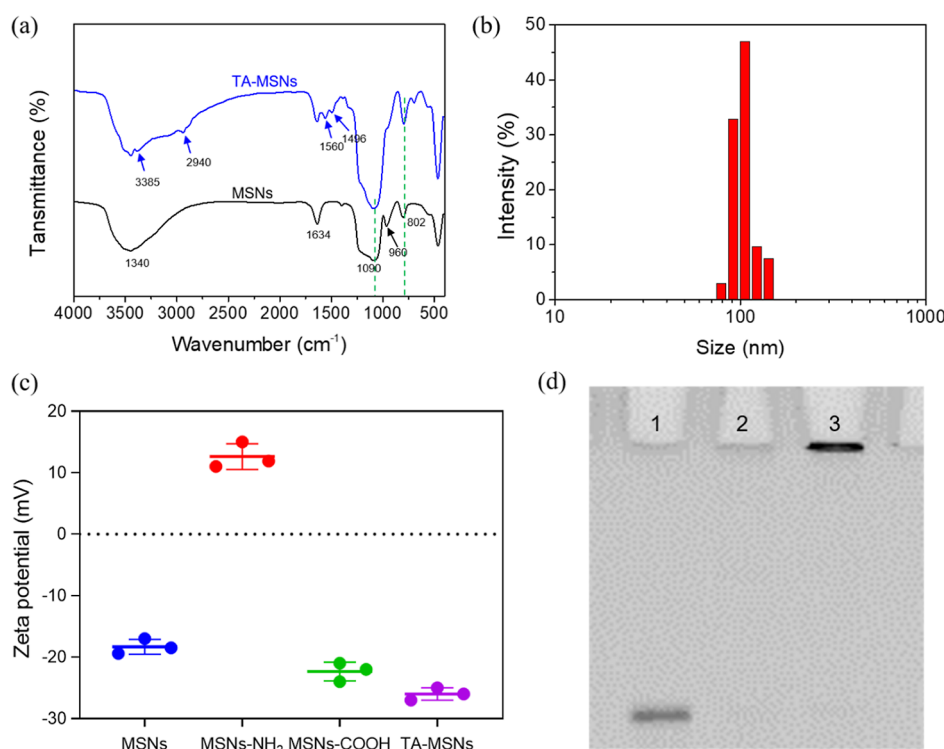
Figure 3. Structural characterization of TA-MSNs. (a) FT-IR spectra of MSNs (black curve) and TA-MSNs (blue curve). (b) Dynamic light scattering measurement of TA-MSNs. (c) Zeta potential measurement of nanoparticles. (d) Polyacrylamide gel electrophoresis image, Lane 1: TfR aptamer, Lane 2: MSNs, Lane 3: TA-MSNs.

plates for 24 h. FITC@MSN, FITC@RS-MSN, and FITC@TA-MSN samples were added into the dish to make the final concentrations of 0, 10, 50, 100, and 200 μg/mL, and the samples were incubated with cancer cells for 4 h. After incubation, the cells were washed with PBS three times, trypsinized with pancreatin, centrifuged at 1000 rpm, and finally resuspended in 500 μL of PBS. The resuspended cells were analyzed on CytoFLEX (Beckman) with a minimum number of 1.0×10^4 cells/per sample. FlowJo (V 10) software was used for data analysis.

2.12. Cell Cytotoxicity Assay. Cell cytotoxicity of the nanoparticles was evaluated by a thiazolyl blue tetrazolium bromide (MTT) colorimetric assay in MCF-7 lines. Cells were cultivated in 96-well culture plates at a density of 1.0×10^4 cells/well. After 24 h, the cells were incubated with different samples for 24 and 48 h at different concentrations, followed by PBS washing three times. After that, cells were exposed to 20 μL of an MTT solution (5 mg/mL in DMSO) with 180 μL of the fresh media and incubated at 37 °C for 4 h. Removing the media, the generated formazan was resuspended in 150 μL of DMSO for absorbance measurements with a spectrometer (Thermo Scientific Varioskan LUX). All experiments were conducted in triplicate. The relative cell viability (%) was expressed as a percentage relative to the untreated control cells.

3. RESULTS AND DISCUSSION

3.1. Characterization of MSNs. MSNs were prepared and purified according to the Stöber method,[42] and the structural features were characterized and analyzed by scanning electron microscopy (SEM) and transmission electron microscopy (TEM). As shown in Figure 2a,b, MSNs retained a uniform spherical morphology and a highly ordered mesoporous structure with a dry particle size of approximately 91.6 nm.

Dynamic light scattering measurement showed that the hydrodynamic diameter of MSNs was 96 ± 10 nm (Figures 2c and S1). The N$_2$ adsorption/desorption isotherm measurement exhibited a type IV isotherm characteristic of mesoporous materials (Figure 2d) and gave a large surface area and pore volume (Table S1). Barrett−Joyner−Halenda showed a thin pore size of about 2.5 nm (Figure 2e). The X-ray diffraction (XRD) measurement displayed a broad diffraction peak at $2\theta = 22°$, which confirmed the amorphous structure of MSNs. Also, its amorphous structure was unaffected by surface group modification, which is consistent with the previous results[43] (Figure 2f).

3.2. Characterization of TA-MSNs. The TA was conjugated to carboxyl-modified MSNs through typical amidation.[44] The synthesized TA-MSNs were analyzed by FT-IR spectroscopy; as shown in Figure 3a, the characteristic absorption peaks of silica were observed at 1090 and 802 cm^{-1} belonging to asymmetric vibrations and symmetric stretching of Si−O−Si and stretching vibrations of Si−OH groups at 960 cm^{-1}, which were consistent with previous reports.[45] The peaks at 3440 and 1634 cm^{-1} indicated that water physically absorbed on the surface of the MSNs. In addition to these inherent absorption peaks mentioned above, new absorption peaks at 1496, 1560, 2940, and 3385 cm^{-1} were assigned to C=O, C=C, and C−H stretching vibration in the DNA molecules for the TA-MSN sample. Notably, the characteristic peak of Si−OH mostly disappeared after multiple steps of surface reaction. Additionally, after TA conjugation, the hydration particle size was increased to 102 ± 8 nm (Figures 3b and S2). Zeta potential measurements indicated that MSNs were negatively charged (−18.3 ± 1.3 mV) and became slightly positively charged (12.6 ± 2.1 mV) after the amine modification. The nanoparticles became highly negatively
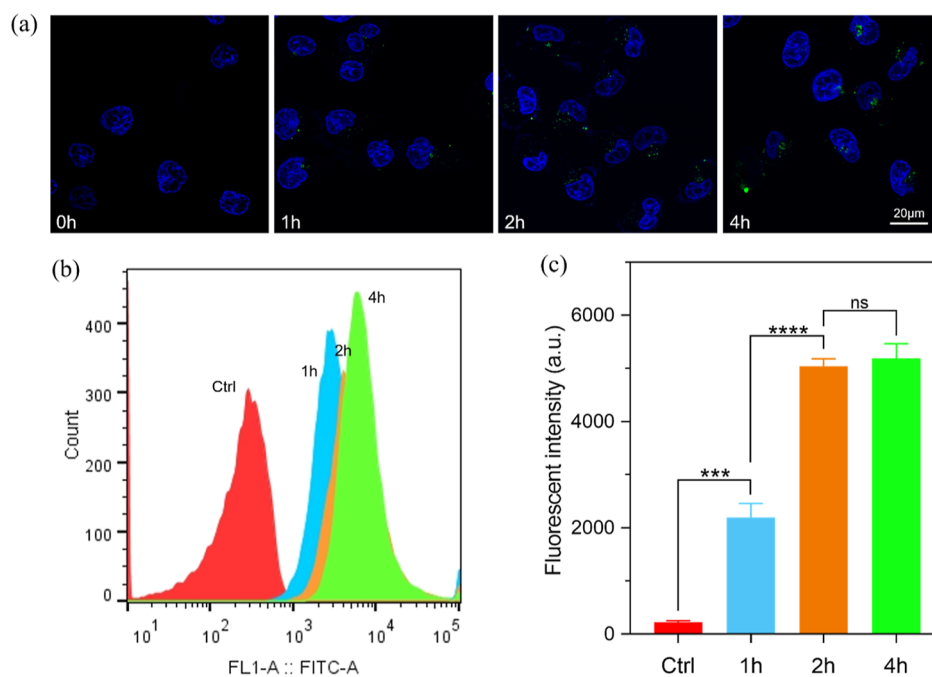
Figure 4. Cellular uptake studies of MSNs. Confocal laser scanning microscopy images (a) and flow cytometry analysis (b) of MCF-7 cells incubated with FITC-loaded MSNs with different incubation times (0, 1, 2, 4 h). (c) Histogram of the fluorescence intensity from flow cytometry analysis. Data represent the mean ± SD of three independent experiments, *$p < 0.05$, **$p < 0.01$, ***$p < 0.001$, ****$p < 0.0001$, ns represents no significant difference.

charged again after surface modification with the carboxyl group (-22.3 ± 1.6) and conjugation with TA (-26.0 ± 1.0 mV) in PBS buffer (Figure 3c). To visually prove TA conjugation on MSNs, polyacrylamide gel electrophoresis was performed. As shown in the gel electrophoresis image of Figure 3d, free TA migrated to the positive electrode (Lane 1), while TA-MSNs remained practically at the origin because of their large size (Lane 3). Furthermore, TA-MSN samples were stained by nucleic acid dye (Lane 3), while MSNs were not (Lane 2), further indicating the successful conjugation of the transferrin receptor aptamer to MSNs.

3.3. Cellular Uptake of MSNs. The cellular uptake of MSNs was studied by using confocal microscopy. First, fluorescence properties of bare MSNs, FITC-loaded MSNs, and FITC-loaded TA-MSNs were measured using a fluorescence spectrophotometer. At the same nanocarrier concentration, the FITC-loaded nanocarriers showed a strong and similar fluorescence emission, whereas the bare MSNs did not (Figure S3). Then, FITC-loaded MSNs (100 μg/mL) were incubated with the model cell MCF-7 to investigate the cellular internalization. As shown in the confocal images of Figure 4a, a gradual increase in intracellular fluorescence intensity with increasing incubation time was observed (Figure S4). Subsequently, flow cytometry was used to quantitatively characterize intracellular fluorescence intensity for different incubation times (Figure 4b), in which the fluorescence intensities of 1 and 2 h incubation were, respectively, 9.7- and 22.2-fold than that of control cells. Also, there was no significant difference between 4 and 2 h incubation (Figure 4c). These results indicated that the MSNs were internalized by MCF-7 cells within a short time, which provide favorable conditions for drug loading and delivery.

3.4. Cellular Uptake of Nanoparticles by Different Cancer Cells. Cell surface receptors are largely involved in controlling cellular processes and are also important targets for

specific recognition and binding.[46] To evidence the decisive role of aptamer functionalization in the binding of TfR on the cancer cell surface, the cellular uptake efficiencies of MSNs, TA-MSNs, and random sequence DNA-modified MSNs (RS-MSNs) were compared in vitro using three human cancer cell lines. MCF-7, HeLa, and A549 cells were, respectively, incubated with FITC-loaded MSNs, TA-MSNs, and RS-MSNs (MSNs' concentration of 100 μg/mL) for 4 h. Fluorescence microscopy images revealed that the TA-MSN group showed higher binding and internalization than the other two groups in three cancer cell lines (Figure 5a,d,g). Afterward, the cellular uptake efficiencies of the three samples were analyzed and compared using flow cytometry, and the results were consistent with fluorescence imaging (Figure 5b,e,h). From Figure 5c,f,i, quantitative data exhibited that the fluorescence intensity of the TA-MSN group was 5.1 times that of MSNs toward MCF-7 cells, 3.9 times toward HeLa cells, and 4.3 times toward A549 cells; however, there were no significant differences between MSNs and RS-MSNs in three cells lines, thereby confirming the role of the specific aptamer in cell targeting, as proposed. In addition, colocalization experiments showed that almost all nanoparticles were present in lysosomes after 4 h of incubation, while most nanoparticles escaped from lysosomes after 10 h of incubation (Figure S5). In summary, TA-functionalized MSNs were more easily taken up into cancer cells by specifically targeting and binding to surface-overexpressed transferrin receptors, which makes them applicable to a wider range of cancer cells.

3.5. Drug Loading and Release. MSNs have abundant mesoporous cavities for drug loading,[47] and they undergo the disintegration process accompanied by drug release at low pH, as reported by Tang and Yao et al.[48,49] Herein, Dox loading at pH 7.4 and in vitro release at three clinically relevant pH of 5.4, 6.4, and 7.4 of TA-MSNs were performed. The Dox loading efficiency in TA-MSNs reached 60.3% within 24 h
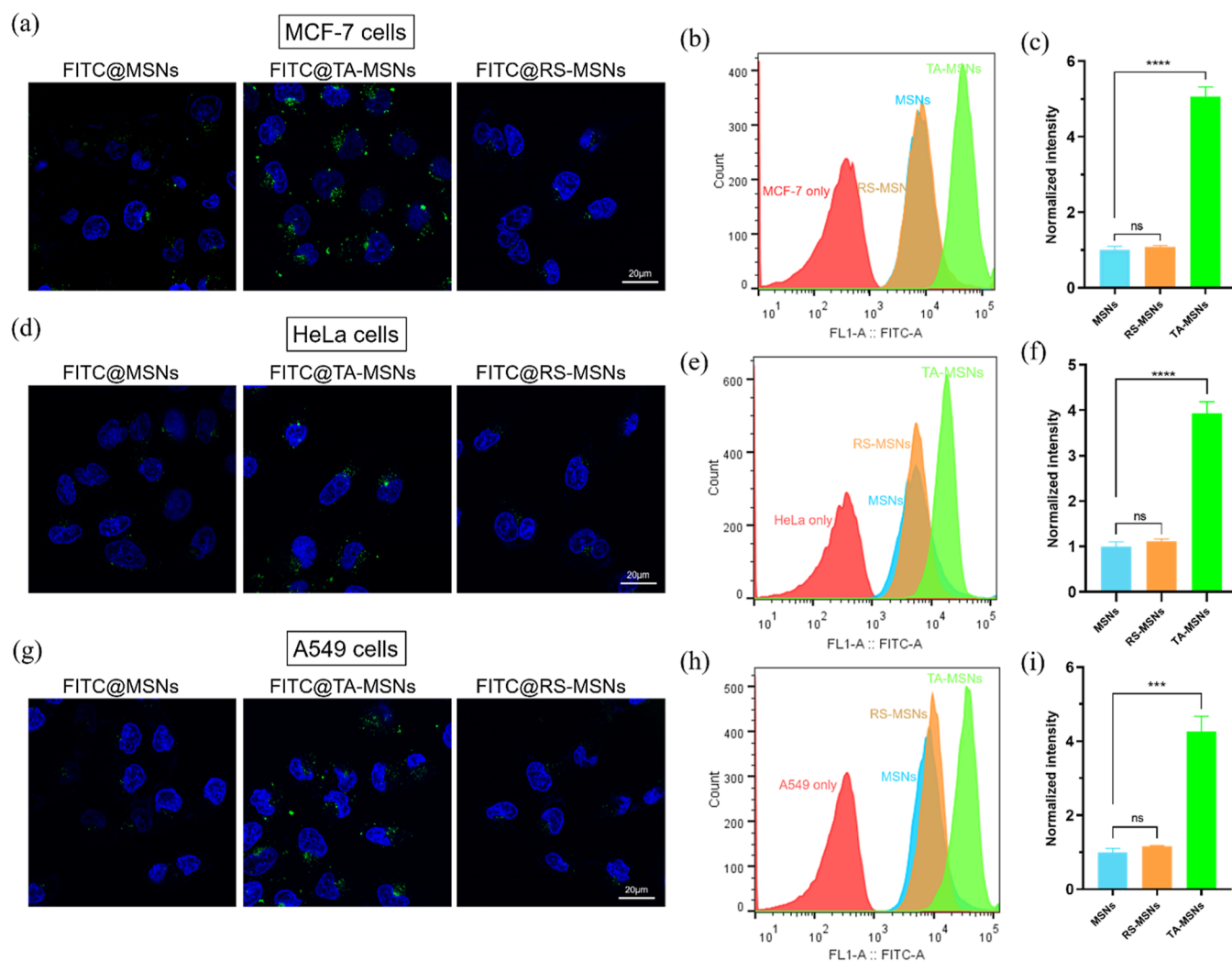
Figure 5. Cellular uptake of MSNs, RS-MSNs, and TA-MSNs in different cancer cell lines. Merged confocal laser scanning microscopy images of MCF-7 (a), HeLa (d), A549 (g) cells, respectively, incubated with FITC-loaded MSNs (left), TA-MSNs (middle), and RS-MSNs (right) for 4 h. The nuclei were stained with Hoechst33342 (blue), and the nanoparticles were decorated by FITC (green). Flow cytometry analysis of MCF-7 (b), HeLa (e), A549 (h) cells, respectively, incubated with FITC-loaded MSNs, RS-MSNs, and TA-MSNs for 4 h. Normalized fluorescence intensity histogram comparison from flow cytometry data toward MCF-7 (c), HeLa (f), A549 (i) cells. The fluorescence intensity of FITC-loaded MSNs in cells was normalized as one. Data represent the mean ± SD of three independent experiments, $*p < 0.05$, $**p < 0.01$, $***p < 0.001$, $****p < 0.0001$.
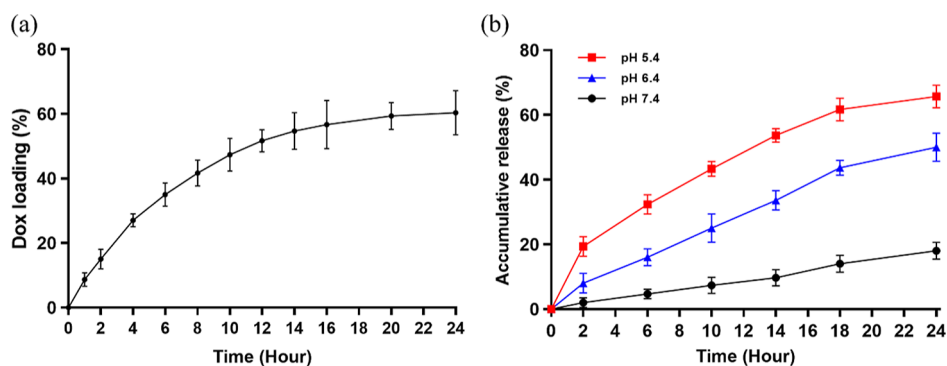

Figure 6. (a) Dox loading rate for different times at pH 7.4. (b) In vitro drug release at different pH and different times. All experiments were performed with three independent experiments.

(Figure 6a); meanwhile, it displayed loading trends and efficiency similar to FITC (Figure S6a). The accumulated drug release reached 65.7% at pH 5.4 within 24 h but only 18.0% at pH 7.4 and 50.0% at pH 6.4 (Figure 6b). Furthermore, in vitro release experiments were conducted for a longer period of up to 3 days, during which more drugs were released. The

accumulative Dox release was 76.3% at pH 5.4 and 70.3% at pH 6.4, whereas it was only 20.0% at pH 7.4 after 3 days (Figure S6b). These contrasts indicated that TA-MSNs were able to maintain a relatively intact structure in the extracellular physiological environment without premature drug leakage but rapidly degrade and release drugs in a low pH environment, which were related to the tumor microenvironment and the intracellular lysosomal environment.

3.6. Cell Viability Assay.

The cytotoxicity of MSNs and TA-MSNs to MCF-7 cells with different concentrations was first measured by an in vitro MTT assay. The results displayed that MSNs and TA-MSNs exhibited negligible toxicity toward MCF-7 cells at high concentrations up to 200 μg/mL with 24 h of incubation (Figure S7). Next, the cytotoxicities of Dox@MSNs, Dox@TA-MSNs, and free Dox were assessed on MCF-7 cells with 24 and 48 h of incubation. As shown in Figure 7a,b, cell viability was time- and concentration-dependent, and
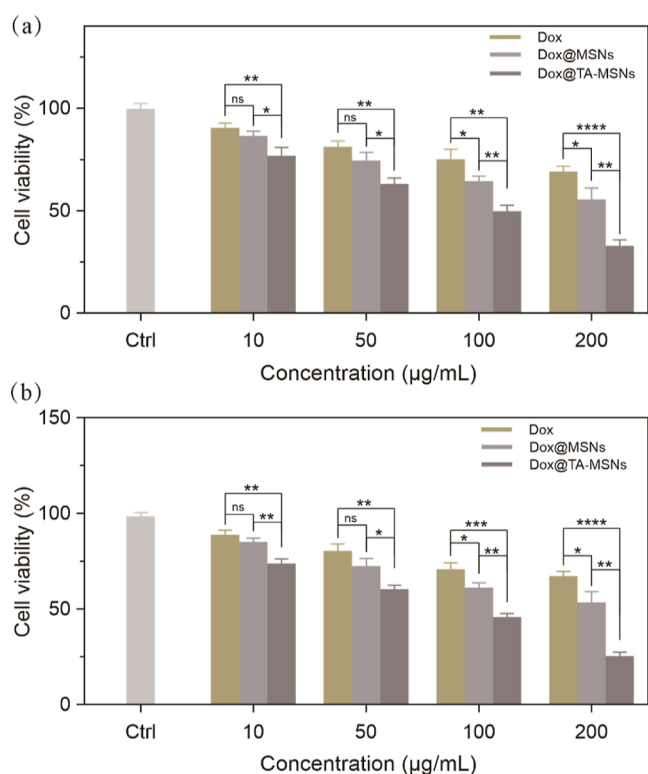

Figure 7. MCF-7 cell viability after 24 (a) and 48 h (b) of incubation with free Dox, Dox@MSNs, and Dox@TA-MSNs at different concentrations. Data represent the mean ± SD of three independent experiments, *$p < 0.05$, **$p < 0.01$, ***$p < 0.001$, ****$p < 0.0001$, ns represents no significant difference.

Dox@TA-MSNs exhibited significantly greater cytotoxicity. At low concentrations of 10 and 50 μg/mL, there were no significant differences in cytotoxicity between Dox and Dox@MSNs; however, the Dox@TA-MSN group was significantly more cytotoxic than the other two groups. Comparing Dox@MSN and Dox@TA-MSN groups, cell viabilities were 86.3 and 76.7% at 10 μg/mL, respectively, and 74.3 and 63.0% at 50 μg/mL, thereby indicating more internalization of Dox@TA-MSNs. At high concentrations of 100 and 200 μg/mL, both Dox@MSNs and Dox@TA-MSNs displayed stronger cytotoxicity compared to free Dox. The cell viabilities of Dox@TA-MSNs were found to be 49.6% compared to 64.3% (Dox@

MSNs) and 74.9% (Dox) at 100 μg/mL, and 32.7% compared to 55.3% (Dox@MSNs) and 69.0% (Dox) at 200 μg/mL, respectively. These comparisons indicate the good delivery efficacy of the TA-MSN nanocarrier, and it can be speculated that the enhanced therapeutic efficacy and significant toxicity of Dox@TA-MSNs are attributed to the TA-mediated effective internalization, which will be promising nanoanticancer agents for targeted cancer therapy.

4. CONCLUSIONS

Functional modification of MSNs using aptamers is one of the most feasible strategies to improve the targeting ability and cellular uptake efficiency. In this study, we demonstrated that the targeting and cellular uptake of TA-modified MSNs were more significantly enhanced compared to those of unmodified and random sequence-modified MSNs, as evidenced by MCF-7, HeLa, and A549 cancer cell lines. Also, the MTT test further showed that Dox-loaded TA-MSNs exhibited a higher cytotoxicity than Dox-loaded MSNs and free Dox. From the above results, it can be seen that TA-functionalized MSNs have enormous application potential in targeted delivery. This study is the first attempt to modify the transferrin receptor aptamer on the surface of MSNs to improve drug delivery efficiency. In contrast to previously reported transferrin-modified mesoporous silica, based on flow cytometry data,[40] TA-modified MSNs were more likely to be internalized by cancer cells. More importantly, aptamers are cheaper and more chemically stable, which can greatly reduce the cost of targeted nanocarriers and make them more valuable in clinical applications. The preceding advantages lead us to believe that this method promises to be a highly efficient yet low-cost strategy for use in targeted therapies for more cancer cells.

■ ASSOCIATED CONTENT

Ⓢ Supporting Information

The Supporting Information is available free of charge at https://pubs.acs.org/doi/10.1021/acsomega.3c06562.

> Hydrated particle size of MSNs, BET, Hydrated particle size of TA-MSNs, fluorescence intensity, CLSM images of MCF-7 cells, FITC loading and drug release, and cytotoxicity of MSNs with different concentrations (PDF)

■ AUTHOR INFORMATION

Corresponding Authors

Xiuhui Tang − *School of Electrical and Information Engineering, Wuhan Institute of Technology, Wuhan 430205, China;* Email: tangxiuhui@163.com

Xuemei Xu − *Key Laboratory for Green Chemical Process of Ministry of Education, Hubei Key Lab of Novel Reaction & Green Chemical Technology, School of Chemical Engineering and Pharmacy, Wuhan Institute of Technology, Wuhan 430205, China;* ⓞ orcid.org/0009-0009-3480-1424; Email: xuxuemei@wit.edu.cn

Authors

Jiajia Zhang − *School of Nursing and Health Management, Wuhan Donghu University, Wuhan 430212, China; Key Laboratory for Green Chemical Process of Ministry of Education, Hubei Key Lab of Novel Reaction & Green Chemical Technology, School of Chemical Engineering and*

Pharmacy, Wuhan Institute of Technology, Wuhan 430205, China

Jing Shang — Key Laboratory for Green Chemical Process of Ministry of Education, Hubei Key Lab of Novel Reaction & Green Chemical Technology, School of Chemical Engineering and Pharmacy, Wuhan Institute of Technology, Wuhan 430205, China

Complete contact information is available at:
https://pubs.acs.org/10.1021/acsomega.3c06562

Author Contributions

Z.J.J. designed the strategy and fabricated the MSNs, RS-MSNs, and TA-MSNs. Z.J.J. and S.J. tested the properties of MSNs and all instrumental characterization. Z.J.J. conducted the cell experiments and analyzed all data. Z.J.J. wrote the manuscript with contributions from all authors. T.X.H. and X.X.M. supervised the project and modified the manuscript.

Notes

The authors declare no competing financial interest.

■ REFERENCES

(1) Bray, F.; Ferlay, J.; Soerjomataram, I.; Siegel, R. L.; Torre, L. A.; Jemal, A. Global cancer statistics 2018: GLOBOCAN estimates of incidence and mortality worldwide for 36 cancers in 185 countries. *Ca-Cancer J. Clin.* **2018**, *68*, 394−424.

(2) Siegel, R. L.; Miller, K. D.; Fuchs, H. E.; Jemal, A. Cancer Statistics, 2021. *Ca-Cancer J. Clin.* **2021**, *71*, 7−33.

(3) Muhamad, N.; Plengsuriyakarn, T.; Na-Bangchang, K. Application of active targeting nanoparticle delivery system for chemotherapeutic drugs and traditional/herbal medicines in cancer therapy: a systematic review. *Int. J. Nanomed.* **2018**, *13*, 3921−3935.

(4) Dutt, Y.; Pandey, R. P.; Dutt, M.; Gupta, A.; Vibhuti, A.; Vidic, J.; Raj, V. S.; Chang, C. M.; Priyadarshini, A. Therapeutic applications of nanobiotechnology. *J. Nanobiotechnol.* **2023**, *21* (1), 148.

(5) Ng, C. T.; Baeg, G. H.; Yu, L. E.; Ong, C. N.; Bay, B. H. Biomedical Applications of Nanomaterials as Therapeutics. *Curr. Med. Chem.* **2018**, *25*, 1409−1419.

(6) Chen, G.; Roy, I.; Yang, C.; Prasad, P. N. Nanochemistry and Nanomedicine for Nanoparticle-based Diagnostics and Therapy. *Chem. Rev.* **2016**, *116*, 2826−2885.

(7) Moholkar, D. N.; Kandimalla, R.; Gupta, R. C.; Aqil, F. Advances in lipid-based carriers for cancer therapeutics: Liposomes, exosomes and hybrid exosomes. *Cancer Lett.* **2023**, *565* (216220), 216220.

(8) Shin, Y. B.; Choi, J. Y.; Shin, D. H.; Lee, J. W. Anticancer Evaluation of Methoxy Poly(Ethylene Glycol)-b-Poly(Caprolactone) Polymeric Micelles Encapsulating Fenbendazole and Rapamycin in Ovarian Cancer. *Int. J. Nanomed.* **2023**, *18*, 2209−2223.

(9) Valente, K. P.; Suleman, A.; Brolo, A. G. Exploring Diffusion and Cellular Uptake: Charged Gold Nanoparticles in an in Vitro Breast Cancer Model. *ACS Appl. Bio Mater.* **2020**, *3*, 6992−7002.

(10) Wang, J.; Ma, Q.; Wang, Y.; Li, Z.; Li, Z.; Yuan, Q. New insights into the structure-performance relationships of mesoporous materials in analytical science. *Chem. Soc. Rev.* **2018**, *47*, 8766−8803.

(11) Horcajada, P.; Gref, R.; Baati, T.; Allan, P. K.; Maurin, G.; Couvreur, P.; Férey, G.; Morris, R. E.; Serre, C. Metal-organic frameworks in biomedicine. *Chem. Rev.* **2012**, *112*, 1232−1268.

(12) Zeng, Y.; Nixon, R. L.; Liu, W.; Wang, R. The applications of functionalized DNA nanostructures in bioimaging and cancer therapy. *Biomaterials* **2021**, *268* (120560), 120560.

(13) Zhang, X.; Zhang, H.; Gu, J.; Zhang, J.; Shi, H.; Qian, H.; Wang, D.; Xu, W.; Pan, J.; Santos, H. A. Engineered extracellular vesicles for cancer therapy. *Adv. Mater.* **2021**, *33*(14)..

(14) von Baeckmann, C.; Guillet-Nicolas, R.; Renfer, D.; Kählig, H.; Kleitz, F. A Toolbox for the Synthesis of Multifunctionalized Mesoporous Silica Nanoparticles for Biomedical Applications. *ACS Omega* **2018**, *3*, 17496−17510.

(15) Vallet-Regí, M.; Schüth, F.; Lozano, D.; Colilla, M.; Manzano, M. Engineering mesoporous silica nanoparticles for drug delivery: where are we after two decades? *Chem. Soc. Rev.* **2022**, *51*, 5365−5451.

(16) Li, Z.; Zhang, Y.; Feng, N. Mesoporous silica nanoparticles: synthesis, classification, drug loading, pharmacokinetics, biocompatibility, and application in drug delivery. *Expert Opin. Drug Delivery* **2019**, *16*, 219−237.

(17) Murugan, C.; Venkatesan, S.; Kannan, S. Cancer Therapeutic Proficiency of Dual-Targeted Mesoporous Silica Nanocomposite Endorses Combination Drug Delivery. *ACS Omega* **2017**, *2*, 7959−7975.

(18) Gangadhar, T. C.; Vonderheide, R. H. Mitigating the toxic effects of anticancer immunotherapy. *Nat. Rev. Clin. Oncol.* **2014**, *11*, 91−99.

(19) Heidari Nia, M.; Koshani, R.; Munguia-Lopez, J. G.; Kiasat, A. R.; Kinsella, J. M.; van de Ven, T. G. M. Biotemplated hollow mesoporous silica particles as efficient carriers for drug delivery. *ACS Appl. Bio Mater.* **2021**, *4*, 4201−4214.

(20) Tang, F.; Li, L.; Chen, D. Mesoporous silica nanoparticles: synthesis, biocompatibility and drug delivery. *Adv. Mater.* **2012**, *24*, 1504−1534.

(21) Shi, Y.; Zhou, M.; Zhang, Y.; Wang, Y.; Cheng, J. MRI-guided dual-responsive anti-tumor nanostructures for synergistic chemo-photothermal therapy and chemodynamic therapy. *Acta Biomater.* **2023**, *158*, 571−582.

(22) Liu, J.; Luo, Z.; Zhang, J.; Luo, T.; Zhou, J.; Zhao, X.; Cai, K. Hollow mesoporous silica nanoparticles facilitated drug delivery via cascade pH stimuli in tumor microenvironment for tumor therapy. *Biomaterials* **2016**, *83*, 51−65.

(23) Chen, F.; Hong, H.; Zhang, Y.; Valdovinos, H. F.; Shi, S.; Kwon, G. S.; Theuer, C. P.; Barnhart, T. E.; Cai, W. In Vivo Tumor Targeting and Image-Guided Drug Delivery with Antibody-Conjugated, Radiolabeled Mesoporous Silica Nanoparticles. *ACS Nano* **2013**, *7*, 9027−9039.

(24) Cao, Y.; Wu, C.; Liu, Y.; Hu, L.; Shang, W.; Gao, Z.; Xia, N. Folate functionalized pH-sensitive photothermal therapy traceable hollow mesoporous silica nanoparticles as a targeted drug carrier to improve the antitumor effect of doxorubicin in the hepatoma cell line SMMC-7721. *Drug Delivery* **2020**, *27*, 258−268.

(25) Xiang, L.; Li, Y.; Gu, X.; Li, S.; Li, J.; Li, J.; Yi, Y. Nucleolin recognizing silica nanoparticles inhibit cell proliferation by activating the Bax/Bcl-2/caspase-3 signalling pathway to induce apoptosis in liver cancer. *Front. Pharmacol* **2023**, *14*, 1117052.

(26) Ghasemii, K.; Darroudi, M.; Rahimmanesh, I.; Ghomi, M.; Hassanpour, M.; Sharifi, E.; Yousefiasl, S.; Ahmadi, S.; Zarrabi, A.; Borzacchiello, A.; Rabiee, M.; Paiva-Santos, A. C.; Rabiee, N. Advances in aptamer-based drug delivery vehicles for cancer therapy. *Biomater. Adv.* **2022**, *140* (213077), 213077.

(27) Salve, R.; Kumar, P.; Chaudhari, B. P.; Gajbhiye, V. Aptamer tethered bio-responsive mesoporous silica nanoparticles for efficient targeted delivery of paclitaxel to treat ovarian cancer cells. *J. Pharm. Sci.* **2023**, *112*, 1450−1459.

(28) Lohiya, G.; Katti, D. S. Carboxylated chitosan-mediated improved efficacy of mesoporous silica nanoparticle-based targeted

drug delivery system for breast cancer therapy. *Carbohydr. Polym.* **2022**, *277* (118822), 118822.

(29) Kumar, P.; Salve, R.; Paknikar, K. M.; Gajbhiye, V. Nucleolin aptamer conjugated MSNPs-PLR-PEG multifunctional nanoconstructs for targeted co-delivery of anticancer drug and siRNA to counter drug resistance in TNBC. *Int. J. Biol. Macromol.* **2023**, *229*, 600−614.

(30) Tang, Y.; Hu, H.; Zhang, M. G.; Song, J.; Nie, L.; Wang, S.; Niu, G.; Huang, P.; Lu, G.; Chen, X. An aptamer-targeting photoresponsive drug delivery system using "off-on" graphene oxide wrapped mesoporous silica nanoparticles. *Nanoscale* **2015**, *7*, 6304−6310.

(31) Lawrence, C. M.; Ray, S.; Babyonyshev, M.; Galluser, R.; Borhani, D. W.; Harrison, S. C. Crystal structure of the ectodomain of human transferrin receptor. *Science* **1999**, *286*, 779−782.

(32) Gammella, E.; Buratti, P.; Cairo, G.; Recalcati, S. The transferrin receptor: The cellular iron gate. *Metallomics* **2017**, *9*, 1367−1375.

(33) Kühn, L. C. The transferrin receptor: a key function in iron metabolism. *Schweiz. Med. Wochenschr.* **1989**, *119*, 1319−1326.

(34) Tortorella, S.; Karagiannis, T. C. Transferrin receptor-mediated endocytosis: a useful target for cancer therapy. *J. Membr. Biol.* **2014**, *247*, 291−307.

(35) Mojarad-Jabali, S.; Mahdinloo, S.; Farshbaf, M.; Sarfraz, M.; Fatahi, Y.; Atyabi, F.; Valizadeh, H. Transferrin receptor-mediated liposomal drug delivery: recent trends in targeted therapy of cancer. *Expert Opin. Drug Delivery* **2022**, *19*, 685−705.

(36) Du, Y.; Wang, Q.; Shi, L.; Li, T. G-Quadruplex-Proximized Aptamers (G4PA) Efficiently Targeting Cell-Surface Transferrin Receptors for Targeted Cargo Delivery. *Nano Lett.* **2022**, *22*, 6328−6333.

(37) Cheng, E. L.; Cardle, I. I.; Kacherovsky, N.; Bansia, H.; Wang, T.; Zhou, Y.; Raman, J.; Yen, A.; Gutierrez, D.; Salipante, S. J.; des Georges, A.; Jensen, M. C.; Pun, S. H. Discovery of a Transferrin Receptor 1-Binding Aptamer and Its Application in Cancer Cell Depletion for Adoptive T-Cell Therapy Manufacturing. *J. Am. Chem. Soc.* **2022**, *144*, 13851−13864.

(38) Zhang, N.; Bing, T.; Shen, L.; Feng, L.; Liu, X.; Shangguan, D. A DNA Aptameric Ligand of Human Transferrin Receptor Generated by Cell-SELEX. *Int. J. Mol. Sci.* **2021**, *22* (16), 8923.

(39) Zhang, N.; Wang, J.; Bing, T.; Liu, X.; Shangguan, D. Transferrin receptor-mediated internalization and intracellular fate of conjugates of a DNA aptamer. *Mol. Ther. Nucleic Acids* **2022**, *27*, 1249−1259.

(40) Ferris, D. P.; Lu, J.; Gothard, C.; Yanes, R.; Thomas, C. R.; Olsen, J. C.; Stoddart, J. F.; Tamanoi, F.; Zink, J. I. Synthesis of biomolecule-modified mesoporous silica nanoparticles for targeted hydrophobic drug delivery to cancer cells. *Small* **2011**, *7*, 1816−1826.

(41) Montalvo-Quiros, S.; Aragoneses-Cazorla, G.; Garcia-Alcalde, L.; Vallet-Regí, M.; González, B.; Luque-Garcia, J. L. Cancer cell targeting and therapeutic delivery of silver nanoparticles by mesoporous silica nanocarriers: insights into the action mechanisms using quantitative proteomics. *Nanoscale* **2019**, *11*, 4531−4545.

(42) Stöber, W.; Fink, A.; Bohn, E. Controlled growth of monodisperse silica spheres in the micron size range. *J. Colloid Interface Sci.* **1968**, *26*, 62−69.

(43) Abburi, A.; Ali, M.; Moriya, P. V. Synthesis of mesoporous silica nanoparticles from waste hexafluorosilicic acid of fertilizer industry. *J. Market. Res.* **2020**, *9*, 8074−8080.

(44) Xu, X.; Zhao, W.; Gao, P.; Li, H.; Feng, G.; Zhao, Z.; Lou, X. Coordination of the electrical and optical signals revealing nanochannels with an 'onion-like' gating mechanism and its sensing application. *NPG Asia Mater.* **2016**, *8* (1), No. e234.

(45) Sakhtianchi, R.; Darvishi, B.; Mirzaie, Z.; Dorkoosh, F.; Shanehsazzadeh, S.; Dinarvand, R. Pegylated magnetic mesoporous silica nanoparticles decorated with AS1411 Aptamer as a targeting delivery system for cytotoxic agents. *Pharm. Dev. Technol.* **2019**, *24*, 1063−1075.

(46) Schlessinger, J. Cell signaling by receptor tyrosine kinases. *Cell* **2000**, *103*, 211−225.

(47) Zhu, C.-L.; Lu, C.-H.; Song, X.-Y.; Yang, H.-H.; Wang, X.-R. Bioresponsive controlled release using mesoporous silica nanoparticles capped with aptamer-based molecular gate. *J. Am. Chem. Soc.* **2011**, *133*, 1278−1281.

(48) Tang, Y.; Teng, Z.; Liu, Y.; Tian, Y.; Sun, J.; Wang, S.; Wang, C.; Wang, J.; Lu, G. Cytochrome C capped mesoporous silica nanocarriers for pH-sensitive and sustained drug release. *J. Mater. Chem. B* **2014**, *2*, 4356−4362.

(49) Xie, X.; Li, F.; Zhang, H.; Lu, Y.; Lian, S.; Lin, H.; Gao, Y.; Jia, L. EpCAM aptamer-functionalized mesoporous silica nanoparticles for efficient colon cancer cell-targeted drug delivery. *Eur. J. Pharm. Sci.* **2016**, *83*, 28−35.